Supporting Information

Integration of organic and inorganic photothermal probes for enhanced photothermometric sensing silver ions

Huiyi Huang,[a,b] Honghong Rao,*[b] Xinyuan Zhang,[a,b] Rongji Wang,[a] Mingming Wei,[a] Xin Xue,[a] Mingyue Luo,[a] Zhonghua Xue*[a], Xiaoquan Lu[a]

[a] *Key Laboratory of Bioelectrochemistry & Environmental Analysis of Gansu Province, College of Chemistry & Chemical Engineering, Northwest Normal University, Lanzhou, 730070 (China)*

[b] *School of Chemistry & Chemical Engineering, Lanzhou City University, Lanzhou, 730070 (China)*

**E-mail address: rhh@nwnu.edu.cn (H. H. Rao); xzh@nwnu.edu.cn (Z. H. Xue).*

Experimental Section

Chemicals and Materials. Citric acid (≥99.5%), iron (III) chloride ($FeCl_3$, ≥98%), potassium ferrocyanide trihydrate ($K_4Fe(CN)_6 \cdot 3H_2O$, ≥99.5%), phosphoric acid (H_3PO_4, ≥85.0%), boric acid (H_3BO_3, ≥99.5%), acetic acid (HAc, ≥99.5%), silver nitrate ($AgNO_3$, ≥99.8%) and 3,3′,5,5′-tetramethylbenzidine (TMB, 98%) were all obtained from Aladdin Chemistry Co., Ltd. (Shanghai, China). Hydrogen peroxide (H_2O_2, 30%) was obtained from Beijing Chemical Corporation (Beijing, China). Superoxide dismutase (SOD) from baker's yeast (S. cerevisiae) was purchased from Sigma-Aldrich Company (Shanghai, China). Sodium hydroxide (NaOH, ≥96%), absolute ethyl alcohol (≥99.7%), tertiary butanol (t-BuOH), sodium bicarbonate ($NaHCO_3$), sodium azide (NaN_3) and other metal salts ($AgNO_3$, $Cr(NO_3)_3$, $Cd(NO_3)_2$, $Ce(NO_3)_2$, $Fe(NO_3)_2$, $Fe(NO_3)_3$, KNO_3, $Mg(NO_3)_2$, $NaNO_3$, $Cu(NO_3)_2$, $Ni(NO_3)_2$, $Pb(NO_3)_2$, $Bi(NO_3)_3$, $Co(NO_3)_2$, $Zn(NO_3)_2$, NH_4NO_3 and $Hg(NO_3)_2$) were purchased from Sinopharm Chemical Reagent (Shanghai, China). The Ag^+ standard solution was purchased from Guobiao (Beijing) Testing & Certification Co. Ltd. All other reagents and chemicals were of at least analytical grade. All aqueous solutions were prepared using deionized (DI) water with a resistivity of 18.24 MΩ·cm. Tap-water samples were collected from the water pipe in our laboratory and Yellow River samples were collected from the local water supply.

Instruments. UV-vis spectra were recorded on a T6 new century spectrophotometer (China). Transmission electron microscopy (TEM) images were obtained on an FEI Tecnai F20 (200 kV) instrument equipped with an Energy dispersive X-ray spectroscopy (EDS). X-ray photo-electron spectroscopy (XPS) was performed by using an ESCALAB 250Xi (Thermo Fisher Scientific, USA). FT-IR spectra were obtained using a Broker Optics FTS3000 spectrometer (DIGI-LAB, USA) in the range of 400-4000 cm^{-1}. Raman spectra were determined by a con focal Raman microscope (Lab RAM HR Evolution, France HORIBA Jobin Yvon S.A.S.). High speed centrifuge (Ke Cheng H3-18K, China) was used for cleaning PB NCs materials. The acidity of the buffer solution was monitored by a Metrohm 632 pH-meter (PHS-3C, China). Homemade constant warm water bath was employed for incubating reaction system. A 2 mL capacity cuvette with a 1cm path length was used for measuring the absorbance, and a diode laser (MDL-H-808-5W-17120005) with output power from 0 to 5W was purchased from Changchun New Industries Optoelectronics Technology Co. Ltd. A pen-style digital thermometer (MITIR-TP677) with a detection range of -50 °C to +300 °C was obtained from a local supermarket. The concentration of Ag^+ in real samples was measured through an ICP-MS spectrometer (NexION 350D, PerkinElmer,

US). The 96-well plates were purchased from Greiner Bio-One. All photographs were taken with a Canon camera (EOS-70D).

Preparation of PB NCs. The PB NCs were synthesized according to recently reported procedure with minor modifications.[1] Briefly, in a standard synthesis, 250 mL of an aqueous solution containing 1 mM $K_4[Fe(CN)_6]$ and 0.5 mM citric acid was firstly prepared under vigorous stirring at 60 °C. Then, a 250 mL mixture of 1 mM $FeCl_3$ and 0.5 mM citric acid was added dropwise to the above solution with a constant voltage funnel under stirring at 60 °C. During the reaction process, a color change from yellow, apple-green, and finally to deep blue was observed. After cooling down to room temperature, a constant stirring of the deep blue solution was maintained at room temperature for another 30 min. Finally, the mixture solution was further centrifuged at 10000 rpm for 1 h to obtain PB NCs precipitation. After being washed with ultrapure water for three times, and redispersed in ultrapure water at a concentration of 0.5 mM to obtain PB NCs solution.

Condition Optimization: To gain an excellent photothermometric sensing performance of Ag^+, experiment conditions containing incubation pH and time between Ag^+ and PB NCs, reaction pH and time of the catalytic system, contents of PB NCs, TMB, H_2O_2 were optimized by using Vis−NIR spectra, respectively. For the optimization of the power and irradiation time of 808 laser, the temperature was recorded using a portable pen-style digital thermometer upon the continuous laser irradiation from 30 s and up to 240 s. The position of the thermometer was fixed in all temperature measurements to avoid temperature variations from position to position. And a small magnet in the cuvette was always stirred at a speed of 800 rpm during the whole irradiation experiment process to avoid detection errors caused by local temperature changes in the temperature test.

Colorimetric and photothermometric sensing of Ag^+ based on the single-signal transduction channel. For the single-signal colorimetric sensing system without TMB, standard procedure for Ag^+ assay was carried out as follows: first of all, 10 μL of Ag^+ with different concentrations (final concentration: 0, 0.3, 0.6, 1, 2, 3, 4, 5, 6, 7, 8, 9 and 10 μM) was respectively incubated with 50 μL of 0.5 mM PB NCs in a disposable cuvette containing 1940 μL of 0.2 M Britton-Robinson (BR) buffer (pH 7.5) at 50 ℃ for 10 min, after cooling to room temperature, the UV-vis spectra and photographs were taken. The same experimental procedure was performed for photothermometric sensing of Ag^+, to measure the uniform temperature of the solution, a small magnet in the cuvette was always stirred at a speed of 800 rpm during the irradiation experiment process. After the above reaction system was irradiated under a 808 nm NIR laser for 120 s, the temperature increase was immediately recorded using a portable pen-style digital thermometer. ΔT ($\Delta T = T - T_0$) was taken as the photothermal signal for each sample, T and T_0 were defined as the temperatures of reaction solution with different Ag^+ concentrations after and before 120 s laser irradiation, respectively. For the single-signal colorimetric sensing system with TMB, the typical Ag^+ analysis was performed as follows: firstly, 10 μL of Ag^+ with different contents (final concentration: 0, 0.3, 0.6, 1, 2, 4, 6, 8, 12, 16, 20, 24 and 28 μM) was respectively mixed with 50 μL of 0.5 mM PB NCs solution in a disposable cuvette containing 240 μL of 0.2 M BR buffer (pH 7.5), and the mixture was incubated at 50 ℃ for 10 min. Then, 1400 μL of 0.2 M BR buffer (pH 4.0) with 200 μL of 10 mM H_2O_2 and 100 μL of 10 mM TMB was added into the above mixture. Subsequently, after the reaction solution was incubated for 10 min at room temperature, its UV-vis spectra and photographs were taken.

Enhanced photothermometric sensing of Ag^+ based on the dual-signal transduction channel. For photothermometric assay, the above reaction solution of the single-signal colorimetric sensing system with TMB was irradiated horizontally upon a 808 nm NIR laser for 120 s at the power of 4 W. Meanwhile, a pen-style digital thermometer was used to record the temperature increase of the above solution along with a small magnet in the cuvette was always stirred at a speed of 800 rpm during the whole irradiation process. ΔT ($\Delta T = T - T_0$) was taken as the photothermal signal for each sample, T and T_0 were defined as the temperatures of reaction solution after and before 120 s laser irradiation, respectively.

Specificity of the Sensing System. The specificity of the explored enhanced photothermal sensing system toward other common cations including Hg^{2+}, NH_4^+, Fe^{3+}, Ce^{2+}, Pb^{2+}, Ni^{2+}, Mg^{2+}, K^+, Bi^{3+}, Na^+, Cu^{2+}, Zn^{2+}, Co^{2+}, Cd^{2+}, Cr^{3+} and Fe^{2+} under the optimal conditions was also investigated, the concentrations of all interfering ions were 20-fold higher than that of silver ions (16 μM).

Detection of Ag^+ in Real Water Samples. For the detection of Ag^+ in real water samples, the Yellow River water samples from three different local water supplies and the tap water sample from the water pipe in our laboratory were filtered three times with a 0.45 μm microfiltration membrane without further pretreatment. Subsequently, the above samples spiked with 1, 5 or 10 μM Ag^+ and 240 μL of 0.2 M BR buffer solution (pH 7.5) containing PB NCs (50 μL) were incubated at 50 ℃ for 10 min, then 1700 μL of 0.2 M BR buffer solution (pH 4.0) containing H_2O_2 (200 μL) and TMB (100 μL) was added into the above solution and left to react for another 10 min. Finally, the spiked samples were analyzed by the proposed enhanced photothermometric method and ICP-MS.

Optimization of the experimental conditions. To investigate the sensing performance of the proposed enhanced photothermometric assay for Ag^+, the solution color, Vis-NIR spectra, and PTEs of the reaction systems with different experimental concentrations were studied in detail. Some factors influencing the sensing performance were firstly evaluated, such as incubation pH and time between Ag^+ and PB NCs, reaction pH and time of the catalytic system, contents of PB NCs, TMB, H_2O_2. The maximum increment of absorbance (A_0-A) shown in Fig. S5 and S6 that could represent TMBox indicator was chosen as the criterion to optimize above factors, in which A_0 and A are the absorbance at 653 nm of the reaction system in the absence and presence of Ag^+. The optimal conditions for Ag^+ detection were found to be (i) a pH value of 7.5 and a time of 10 min for the incubation of Ag^+ with PB NCs, (ii) a pH value of 4.0 and a time of 10 min for the catalytic reaction, (iii) 12.5 μM PB NCs, 0.5 mM TMB, and 1 mM H_2O_2. With this optimized condition, a sensitive Ag^+ content-dependent color change was successfully observed. For the optimal power and irradiation time of 808 laser, as displayed in Fig. S7A, the temperature increase of the reaction system at different irradiation powers of 808 laser indicated that 4 W is practicable. Moreover, under the irradiation power of 4 W, the system temperature increased dramatically with the increasing PB NCs contents at different irradiation times. As clearly, the temperature increase at 120 s displays the best linear relationship with PB NCs contents in the range of 5~12.5 μM (Fig. S7B), which is more useful for fabricating thermometer readout-based quantitative strategy. Thus, 120 s was used as an optimal irradiation time to obtain a sensitive temperature change in the subsequent Ag^+ analysis.

Feasibility of the enhanced photothermometric sensing of Ag^+ based on the dual-signal transduction channel. To further investigate the sensing performance of the dual-signal

transduction channel for enhanced photothermometric assay of Ag^+, the UV-vis spectra and photothermal testing of different components were studied in detail. As shown in Fig. S8A, in the absence of Ag^+, PB NCs solution exhibited a maximum absorbance at 712 nm with a distinguishable blue color (12.5 μM, curve a). After addition of 16 μM Ag^+, the intensities of the blue color and absorbance of PB NCs system decreased significantly (curve c) ascribed to the effective conversion of PB NCs to $Ag_4[Fe(CN)_6]$ nanoparticles (AgFC NPs). Interestingly, with the introduction of TMB, the mixture of PB NCs and TMB−H_2O_2 solution yielded a deep-blue with distinct characteristic peaks of oxTMB at 653 nm and 890 nm (curve d) attributed to the high peroxidase-like activity of PB NCs. However, with the increase of Ag^+ contents (0.3, 4, 16 μM), the PB NCs-TMB-H_2O_2 system showed a gradual fading tendency from blue to light blue and then to nearly colorless along with the changes of UV-vis absorbance with the same trend (curve f, g, e). Furthermore, the corresponding temperature changes of the above colorimetric system were displayed in Fig. S8B. PB NCs solution with the good photothermal effect shows an obvious temperature increase (histogram a) after 120 s irradiation at 808 nm laser. Remarkably, a significant temperature decrease was observed after 16 μM of Ag^+ addition (histogram c) close to that of the TMB−H_2O_2 solution (histogram b). More significantly, a distinct temperature decrease for the dark-blue PB NCs-TMB-H_2O_2 system (histogram d) after the increasing concentration of Ag^+ addition (histogram f, g, e) was observed. All these results indicated that target Ag^+ could not only directly induce PB-to-AgFC conversion to suppress the photothermal response, but also markedly inhibit the peroxidase-like activity of PB NCs to hinder the photothermal response of oxTMB catalyzed by PB NCs nanozyme, and demonstrated the capability of the proposed dual-signal transduction channel for photothermometric sensing Ag^+.

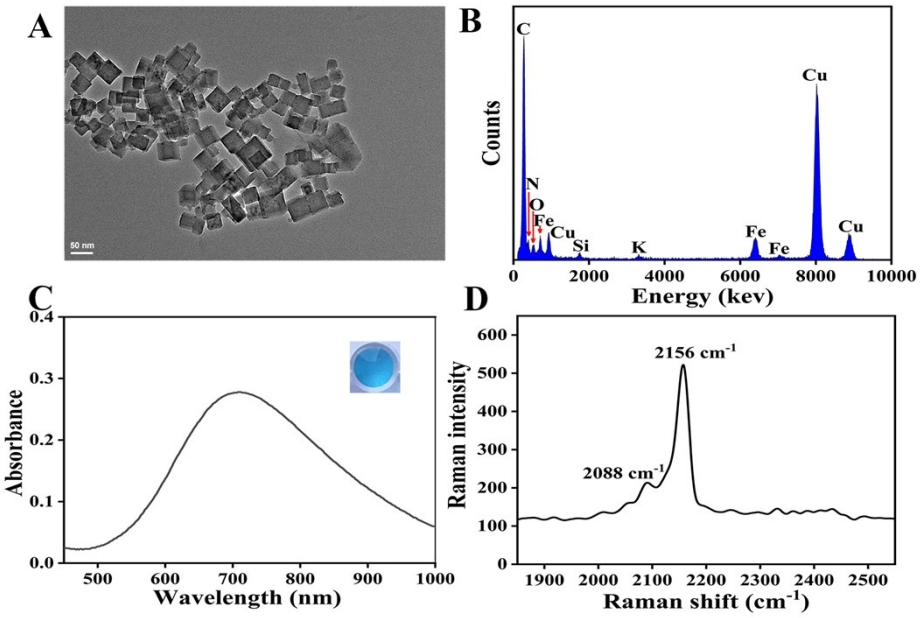

Fig. S1. Characterization of the prepared PB NCs. (A) TEM image. (B) EDS spectrum. (C) UV-vis absorption spectrum and the photo of the solution (inset). (D) Raman spectrum.

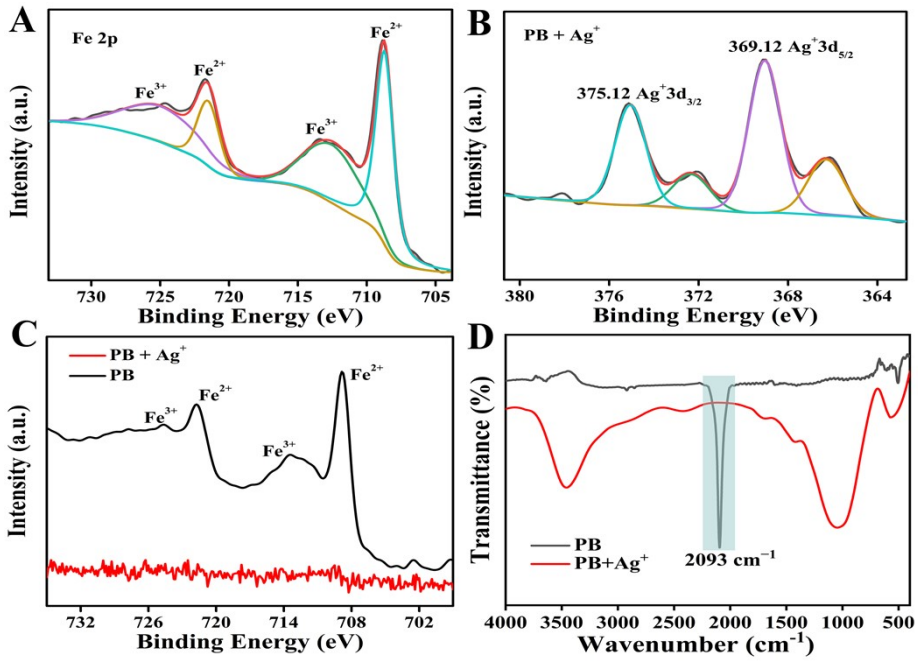

Fig. S2. XPS and FT-IR spectra of the PB NCs before and after incubation with Ag^{+}. (A) Fe 2P XPS spectrum of the PB NCs. (B) Ag 3d XPS spectrum of the PB NCs after incubation with Ag^{+}. (C) XPS survey spectra of both samples. (D) FT-IR spectra of both samples.

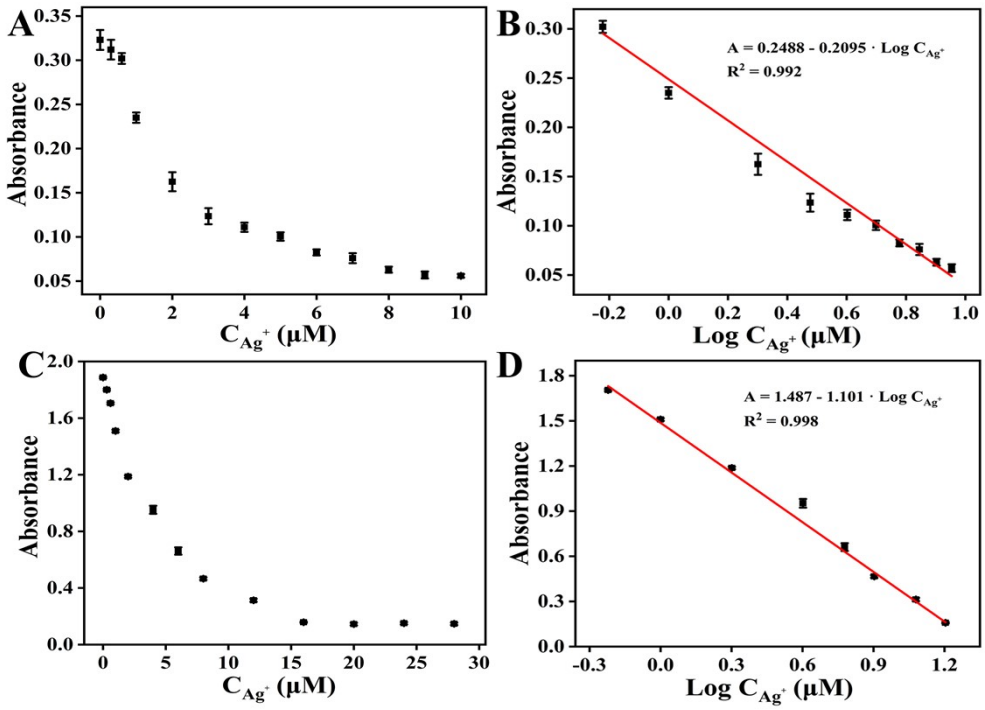

Fig. S3. Absorbance responses of (A) the single-signal colorimetric sensing system without TMB at 712 nm (A_{712}) and (C) with TMB at 653 nm (A_{653}) versus the different Ag^+ concentrations. The linear relationship between (B) A_{712} and (D) A_{653} with the logarithm of Ag^+ concentrations. Error bars indicate standard deviations (n = 3).

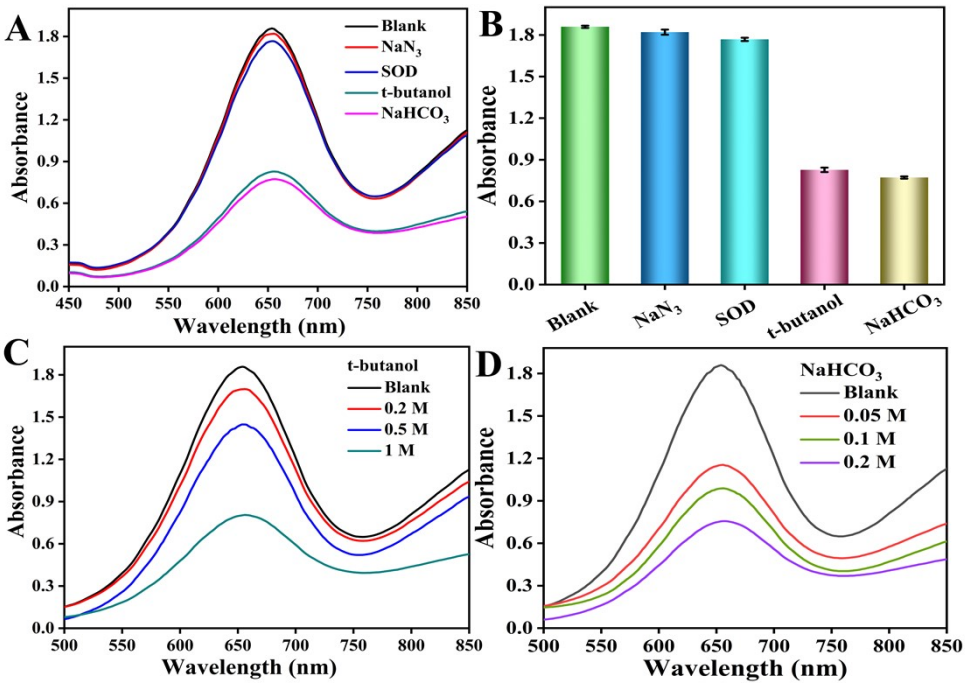

Fig. S4. UV-vis absorption spectra and the corresponding histograms of the catalytic system in the presence of different free-radical scavengers.

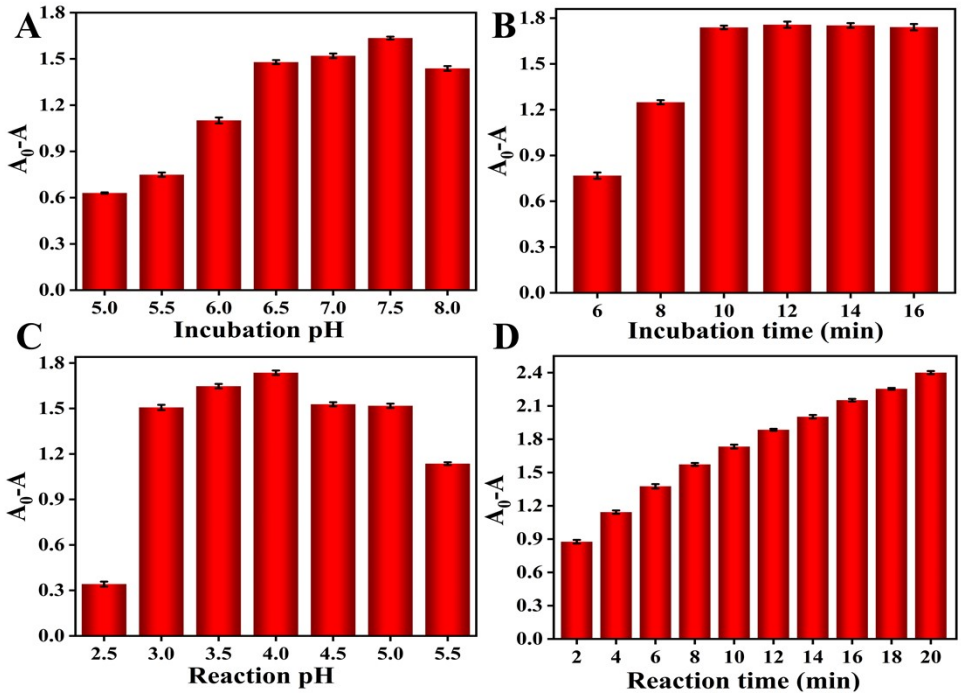

Fig. S5. The effects of different pH and time conditions to the proposed enhanced photothermometric system. (A) Incubation pH and (B) time between Ag^+ and PB NCs. (C) Reaction pH and (D) time of the catalytic system.

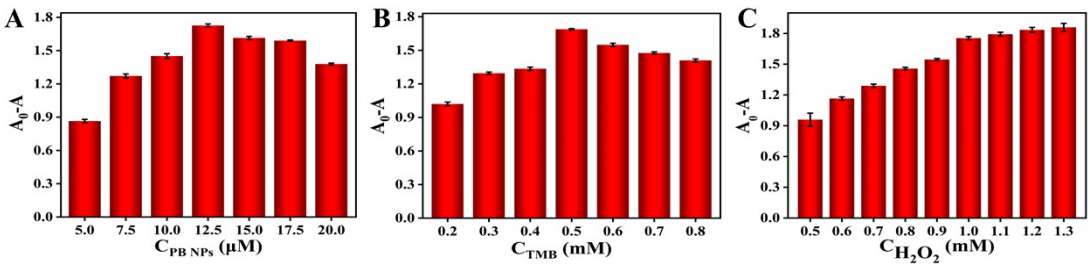

Fig. S6. The effects of different chemicals concentrations to the proposed enhanced photothermometric system. (A) PB NCs. (B) TMB. (C) H_2O_2.

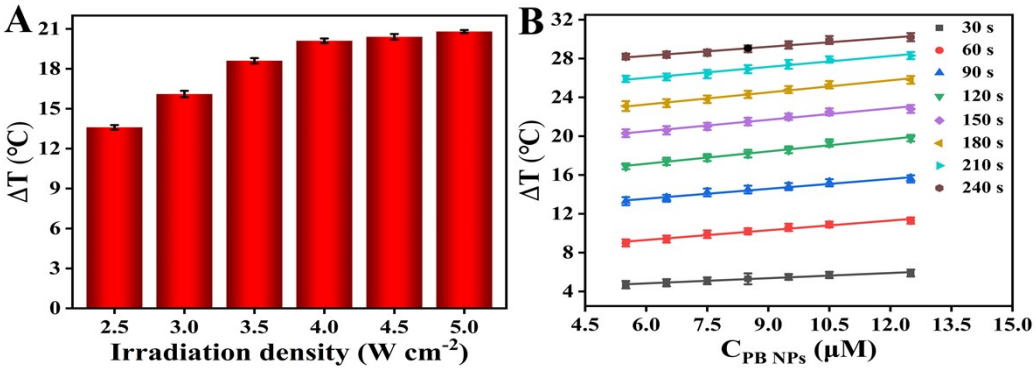

Fig. S7. The effects of different irradiation conditions to the proposed enhanced photothermometric system. (A) Irradiation density. (B) Irradiation time.

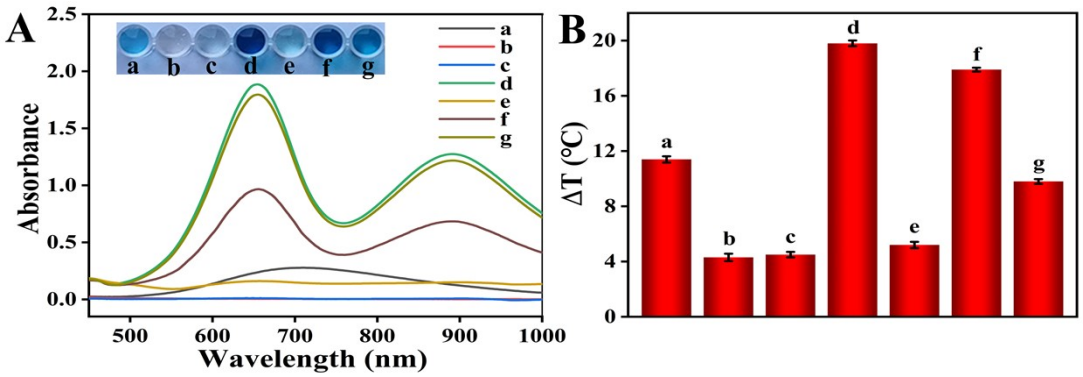

Fig. S8. (A) UV-vis spectra and (B) temperature increase of different components (Insert: corresponding solution color). (a-g: PB NCs; TMB−H_2O_2; 16 μM $AgNO_3$ + PB NCs; PB NCs + TMB−H_2O_2; 16 μM $AgNO_3$ + PB NCs + TMB−H_2O_2; 0.3 μM $AgNO_3$ + PB NCs + TMB−H_2O_2; 4 μM $AgNO_3$ + PB NCs + TMB−H_2O_2)

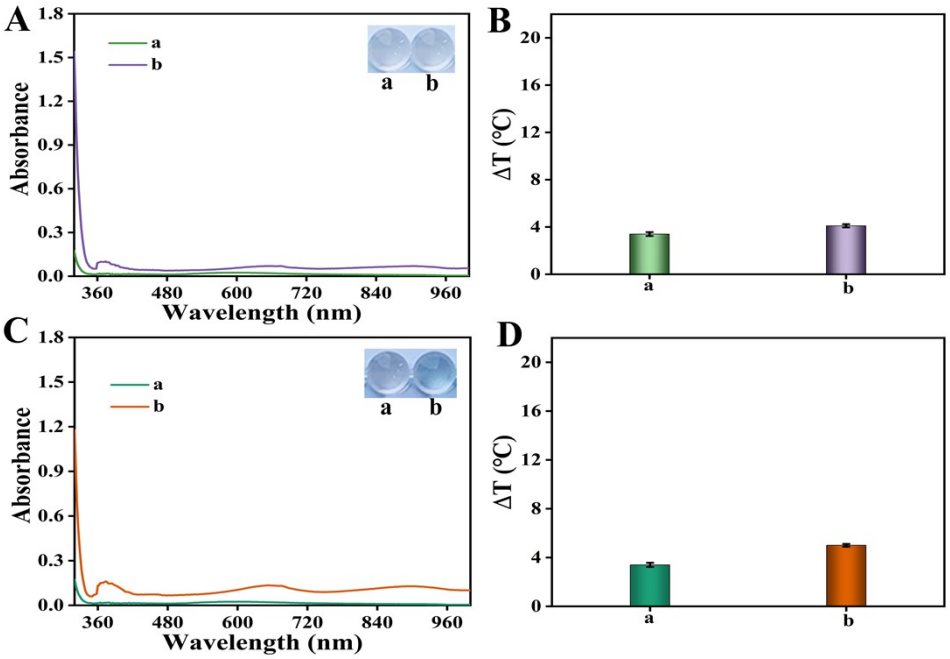

Fig. S9. UV-vis spectra and temperature increase of different reaction solutions (A and B: (a) 10 μM Fe^{3+}, insert of photographs; (b) 10 μM Fe^{3+} + 0.5 mM TMB + 1 mM H_2O_2); (C and D: (a) 10 μM Ag^{+}, insert of photographs; (b) 10 μM Ag^{+} + 0.5 mM TMB + 1 mM H_2O_2).

Table S1. Comparison of the sensing performance of different Ag^+ assays.

Detection Methods	Detection Probes	Linear Range	LOD	Ref.
Colorimetric	BSA-stabilized Au clusters	0.5-10 μM	0.204 μM	[2]
Colorimetric	Pyridine labeled Au NPs	-	1 mM	[3]
Photothermometric	Hydroquinone and Au NPs	1-170 μM	1 μM	[4]
Colorimetric	Tween 20 labeled Au NPs	0.4-1 μM	0.1 μM	[5]
Fluorometric	Metal-organic framework	0-500 μM	0.09 μM	[6]
Paper-based Colorimetric	PB NPs	-	0.9 μM	[7]
Paper-based Colorimetric	Specifically responsive indicators	-	1.69 μM	[8]
Colorimetric	Au NPs	2–28 μM	0.85 μM	[9]
Photothermal Microfluidic	PB NPs	-	0.25 μM	[10]
Enhanced Photothermometric	PB NCs 3,3′,5,5′-tetramethylbenzidine	0.3-20 μM	0.13 μM	This work

Table S2. Determination of Ag^+ in Real Water Samples based on spike method.

samples	spiked (μM)	ICP-MS (μM)	RSD (%)	Enhanced Photothermometric sensing (μM)	RSD (%)	recovery (%)
Yellow River water 1	0	0.02	1.4	ND		
	1	1.05	1.7	1.06	2.2	104
	5	5.02	2.0	4.99	2.9	99.4
	10	10.02	2.3	9.93	3.0	99.1
Yellow River water 2	0	ND		ND		
	1	1.02	1.7	1.03	2.5	103
	5	4.98	2.1	4.95	2.8	99
	10	10.05	2.5	10.01	2.9	100.1
Yellow River water 3	0	0.04	1.1	ND		
	1	1.06	2.1	1.02	2.0	98
	5	5.06	2.0	5.04	3.2	100
	10	10.02	1.8	10.06	4.1	100.2
Tap water	0	0.03	1.5	ND		
	1	1.04	2.0	1.05	2.2	102
	5	5.03	2.6	4.95	3.2	98.4
	10	10.07	2.3	9.93	3.7	99

Note: Recovery (%) = $[(C_{found} - C_{blank})/C_{Added}] \times 100\%$.

RSD (%) = (SD/mean) × 100%

References

1. W. Huang, Y. Liang, Y. Deng, Y. Cai and Y. He, *Microchim. Acta*, 2017, **184**, 2959-2964.
2. Y. Chang, Z. Zhang, J. Hao, W. Yang and J. Tang, *Sens. Actuators B Chem*., 2016, **232**, 692-697.
3. A. Alizadeh, M. M. Khodaei, Z. Hamidi and M. b. Shamsuddin, *Sens. Actuators B Chem*., 2014, **190**, 782-791.
4. B. Liu, H. Tan and Y. Chen, *Microchim. Acta*, 2013, **180**, 331-339.
5. C.-Y. Lin, C.-J. Yu, Y.-H. Lin and W.-L. Tseng, *Anal. Chem*., 2010, **82**, 6830-6837.
6. J.-N. Hao and B. Yan, *J. Mater. Chem. A*, 2015, **3**, 4788-4792.
7. N. Bagheri, S. Cinti, E. Nobile, D. Moscone and F. Arduini, *Talanta*, 2021, **232**, 122474.
8. L. Liu and H. Lin, *Anal. Chem*., 2014, **86**, 8829-8834.
9. A. Selva Sharma, T. SasiKumar and M. Ilanchelian, *J. Clust. Sci*., 2018, **29**, 655-662.
10. G. Fu, Y. Zhu, K. Xu, W. Wang, R. Hou and X. Li, *Anal. Chem*., 2019, **91**, 13290-13296.